Front. Earth Sci. 2023, 17(1): 100−108
https://doi.org/10.1007/s11707-021-0958-x

RESEARCH ARTICLE

P-wave and S-wave response of coal rock containing gas-water with different saturation: an experimental perspective

Dameng LIU (✉)[1,2], Lijing LI[1,2], Zheng ZHAO[1,2], Wei CHEN[3], Yidong CAI[1,2], Yongkai QIU[1,2], Yingfang ZHOU[4]

1 School of Energy Resources, China University of Geosciences, Beijing 100083, China
2 Coal Reservoir Laboratory of Natural Engineering Research Center of CBM Development & Utilization, China University of Geosciences, Beijing 100083, China
3 Beijing Furuibao Energy Technology Company, Beijing 100176, China
4 School of Engineering, King's College, University of Aberdeen, AB24 3UE Aberdeen, UK

Abstract The acoustic response of gas and/or water saturated coal rock is fundamental for establishing the correspondence between the physical properties of the coal reservoir and the characteristics of the well-logging response, which is the technology essential for the geophysical exploration of coalbed methane (CBM). This acoustic response depends on water (S_w) and gas (S_g) saturation among other factors. In this study, we performed acoustic tests on dry and different gas-water saturated coal samples with different degrees of metamorphism and deformation, collected from several coal mining areas in China. These tests enabled us to analyze the influence of coal type and gas-water saturation on the acoustic response of CBM formations. Our results show that the acoustic velocity of P-wave and S-wave (V_p and V_s, respectively), and the relative anisotropy of and V_s, increased with increasing vitrinite reflectance, density, V_p and S_w. With S_w increasing from 0 to 100%, the growth rate of the acoustic velocity decreased with increasing vitrinite reflectance. The V_p/V_s ratio of tectonic coal was generally higher than that of primary coal. The growth rate of the relative anisotropy in tectonic coal was markedly higher than that in primary coal.

Keywords coal rock, gas-water, water saturation, acoustic velocity, relative anisotropy

1 Introduction

Acoustic waves are the propagation of vibrations generated by a sound emitter in a medium. The speed, frequency, and attenuation coefficient of acoustic waves differ for different components, structure, and mechanical properties of the medium. Acoustic wave detection technology is reliable, economical, nondestructive, and provides rapid results (Sharma and Singh, 2008; Khandelwal and Ranjith, 2010). Owing to these advantages, acoustic logging is widely used to identify the geological characteristics of coal reservoirs. By comparing the differences in the acoustic wave propagating through coal samples with a different degree of metamorphism and deformation, or under different stress loads, the effects of metamorphism, density (Morcote et al., 2010; Liu et al., 2017a), deformation degree (Feng et al., 2016; Zhang et al., 2017), mechanical parameters (Khandelwal and Singh, 2009; Khandelwal, 2013; Chen et al., 2017; Zhao et al., 2021), and stress load state (Hou et al., 2020; Zhang et al., 2021) on the acoustic wave velocity and attenuation coefficient have been identified. It has been found that the acoustic wave attenuation coefficient decreases with increasing density and/or degree of coal metamorphism. The P-wave velocity (V_p) correlates positively with the strength and density, and negatively with the degree of deformation or fracture, of the coal rock. Coal reservoir parameters, such as coal seam stability, coal structure, and brittleness index, can thus be identified through acoustic logging data.

With the increasing fervor of coalbed methane (CBM) development (Lupton et al., 2020) and its increasing requirements for detailed reservoirs characterization (Wang et al., 2017; Banerjee and Chatterjee, 2021), coal

Received October 16, 2021; accepted December 16, 2021

E-mail: dmliu@cugb.edu.cn

geologists began to further investigate the application of acoustic testing techniques in CBM exploration and development. The effect of wetting conditions and coal microstructure on acoustic velocity has been investigated through the acoustic testing of coal samples under various conditions of porosity (Li et al., 2017), permeability (Wang et al., 2015), and water saturation (S_w) (Liu et al., 2017b; Wang et al., 2020; Dugarov et al., 2021). The fitting results of V_p with the value of S_w, porosity and permeability of coal samples showed that V_p increased exponentially with increasing S_w in the coal sample, while it correlates negatively with coal porosity and permeability. These results provide an important reference for the evaluation of the physical properties of coal reservoirs from acoustic logging.

Most of the recent research on the application of acoustic testing in the evaluation of coal reservoir characteristics has been conducted on dry coal samples or coal samples with a given S_w. However, since coal reservoirs usually contain mixed-phase, gas, and water fluids (Liu et al., 2020; Liu et al., 2021), the changes in their acoustic response are difficult to interpret. In this work, we conducted acoustic tests of gas-water saturated coal samples with a different degree of metamorphism and deformation to investigate the variation in their acoustic velocity, V_p/V_s, and relative anisotropy. This enabled us to discuss the correlation between the S_w (or S_g) of the coal samples and their acoustic response characteristics. This work fills a gap in current research and provides a further reference for the application of acoustic logging technology in CBM exploration and development.

2 Experimental methods

2.1 Acoustic testing of dry samples

2.1.1 Experimental samples

In this experiment, 8 samples of primary coals and 1 sample of tectonic coal (cataclastic coal with multiple small-scale fractures visible through the coal block), metamorphosed at different degrees, were collected from coal mines in Changji and Fukang on the southern edge of the Junggar Basin and Lvliang, Changzhi, Yangquan, and Gujiao in the Qinshui Basin, China. According to the standard sample size requirements of the International Society for Rock Mechanics (ISRM) Test Committee (Altindag and Güney, 2006), the coal rock was cut along the bedding planes and drilled into cylinders with diameter of 25 mm and length of 50 mm (Fig. 1(a)). Scale paper (with a scale interval of 30°) was attached to the upper and lower sections of the coal sample, and the direction of dip of the coal formation was marked as 0° (Fig. 1(b)). The coal samples were dried in a thermostat for 24 h before the acoustic wave test (thermostat temperature: 50°C). The specific parameters of each coal sample are listed in Table 1.

2.1.2 Ultrasonic P-wave and S-wave testing equipment

The ultrasonic P-wave and S-wave velocity of the coal samples at room temperature (25°C) was measured with the pulse transmission method (Liu et al., 2017b). The experimental setup comprised an oscilloscope, a pulse signal generator, a pair of P-wave probes, a pair of S-wave probes, a pair of aluminum gaskets, and a signal

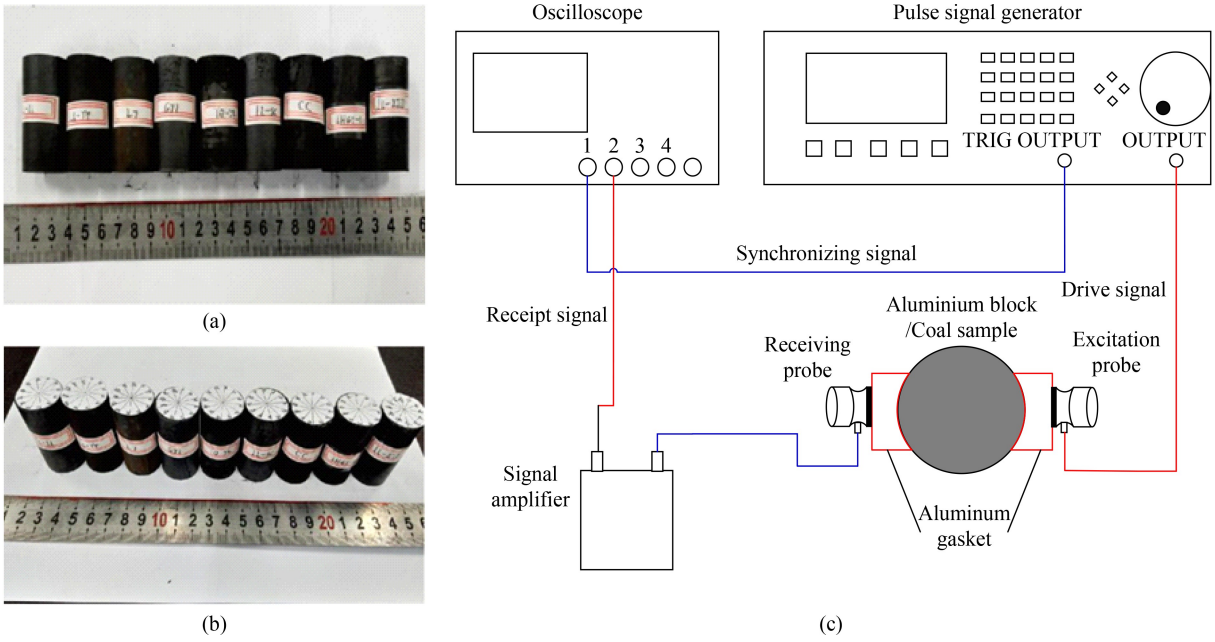

Fig. 1 Coal samples (a) and (b) and ultrasonic P-wave and S-wave testing equipment (c).

Table 1 Basic parameters of selected coals with different vitrinite reflectance

Sample ID	Coal structure	Sampling points	Location	$R_{o,m}$/%	L/mm	D/mm	Density/(g·cm^{-3})	Porosity/%
LHG7-1	Primary coal	Changji	Junggar Basin	0.34	50.36	25.58	1.30	11.08
L7	Primary coal	Fukang		0.71	50.72	25.55	1.32	0.94
LL-LL	Primary coal	Lvliang	Qinshui Basin	1.05	49.57	25.47	1.37	0.99
LL-YT	Primary coal	Lvliang		1.18	50.25	25.47	1.38	1.20
LL-ZJD	Primary coal	Lvliang		1.47	49.50	25.80	1.41	1.56
LL-SC	Primary coal	Lvliang		1.98	50.71	25.64	1.46	5.16
CC	Primary coal	Changzhi		2.04	49.26	25.81	1.47	3.89
YQ-5K	Primary coal	Yangquan		2.54	50.02	25.46	1.53	2.78
GJ	Tectonic coal	Gujiao		1.49	49.02	25.48	1.40	3.18

amplifier (Fig. 1(c)). The dry samples were tested using an ultrasonic low-frequency band (50 kHz–2 MHz). The maximum sampling rate of the P-wave and S-wave broadband ultrasonic transducer was 10 Ms/s.

2.1.3 Acoustic test procedure

1) The instruments were assembled, and the experimental parameters were set.

2) The P-wave excitation probe was connected to the receiving probe with a vaseline coupling agent, to obtain the time of P-wave propagation in the transducer (t_{p0}).

3) A pair of P-wave probes were connected to the upper and lower surfaces of the aluminum block using a vaseline coupling agent. The P-wave propagation velocity in the aluminum block (V'_p) was calculated from the obtained P-wave propagation time, t_{p1}, as follows:

$$V'_p = \frac{L_a}{t_{p1} - t_{p0}}, \tag{1}$$

where L_a is the length of aluminum block, m.

4) Two aluminum gaskets were placed on the two sides of the cylindrical aluminum block, a pair of P-wave probes were placed on the gaskets for P-wave testing (Fig. 1(c)), and the P-wave propagation time, t_{p2}, was recorded. The total time, t_{p3}, of P-wave propagation through the transducer and aluminum gasket was calculated from the P-wave propagation speed in the aluminum block, as follows:

$$t_{p3} = t_{p2} - \frac{D_a}{V'_p}, \tag{2}$$

where D_a is the diameter of aluminum block, m.

5) After replacing the aluminum block between the two aluminum gaskets with a coal sample, the P-wave test was repeated, and the P-wave propagation time, t_{p4}, was recorded. The P-wave propagation velocity, V_p, in the coal sample was calculated as follows:

$$V_p = \frac{D}{t_{p4} - t_{p3}}, \tag{3}$$

where D is the diameter of coal samples, m.

6) Using the marked scale stickers on the sample ends as a reference, the coal sample was rotated 30° counterclockwise for each measurement, and Step 5) was repeated for a total of six times to obtain the V_p of the same coal sample in different directions.

7) After the V_p measurement was completed for each coal sample, the P-wave probes were replaced with the S-wave probes, and Steps 2)–6) were repeated to measure the S-wave velocity (V_s) of the same coal sample in different directions. V_s measurements were performed in all the coal samples, and the experiment was completed.

2.2 Acoustic testing of the saturated coal samples

2.2.1 Displacement experiment

The displacement experiment was conducted using an NSQT70-200 high-temperature, high-pressure, acid-resistant long-core displacement system (Fig. 2). For safety reasons, nitrogen, which has gas properties similar to those of methane, was used in the displacement process. As shown in Fig. 2, a steel pipe connected to a nitrogen cylinder was driven through one end of the coal sample, and a measuring cylinder with a scale was connected to the other end. During the experiment, the S_w in the coal sample was determined by the rising liquid level in the measuring cylinder. The space of the displaced water was occupied by gas, and the corresponding gas saturation (S_g) was obtained. In this experiment, the S_w of the two-phase fluid within the coal sample was set at 0, 20%, 40%, 60%, 80%, and 100% (corresponding S_g values: 100%, 80%, 60%, 40%, 20%, and 0). To avoid damaging the coal sample during the experiment, the experimental setup included an axial pressure of 2 MPa, a confining pressure of 3 MPa, and air pressure of 5 MPa.

2.2.2 Test procedure

1) The dry coal samples were placed in a beaker and were fully submerged in distilled water. The beaker was then placed in a vacuum chamber, and the coal samples were soaked for 8 h.

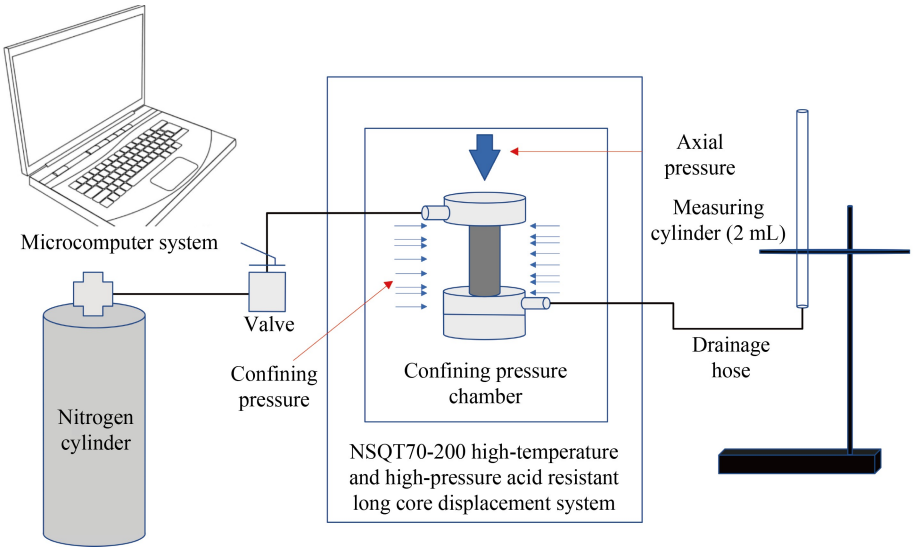

Fig. 2 Schematic diagram of displacement experiment.

2) Under confining pressure, the oil in the instrument cavity can enter the coal sample and affect the accuracy of the experiment. To prevent this, each numbered coal sample was placed on the core seat and wrapped with a heat-shrinkable tube.

3) Thus assembled, the coal sample was placed in the confining pressure chamber. One end of the confining pressure chamber was connected to a nitrogen cylinder; the other end was connected to a drainage hose. The end of the hose was connected to a 2-mL measuring cylinder (Fig. 2).

4) The air in the coal sample base and the drainage hose was emptied to ensure the accuracy of the experiment.

5) The confining pressure chamber was closed, and a confining pressure load of 3 MPa and an axial pressure load of 2 MPa were applied to the coal sample. The confining pressure was loaded by the oil pressure in the confining pressure chamber. The axial pressure was controlled by the two pressure heads at the top and bottom of the coal column.

6) The valve of the nitrogen cylinder was opened, and the gas pressure was gradually adjusted to 5 MPa. This began to displace the water in the coal sample. The changing water level in the measuring cylinder was monitored.

7) The water absorption of the coal sample was calculated from the pore volume, and the rising water level in the measuring cylinder was observed. When the designed displacement was reached, the air valve was closed immediately, and the pressure was released to stop the displacement.

8) After removing the axial pressure and releasing the confining pressure, the coal sample was removed from the confining pressure chamber. The heat-shrinkable tube was then removed from the surface of the coal sample, and the acoustic parameters of the saturated coal sample were tested following the same procedure as that followed for the dry samples. According to the experimental design, the coal sample S_w was set at 100%, 80%, 60%, 40%, 20%, and 0 (corresponding S_g: 0, 20%, 40%, 60%, 80%, and 100%).

9) When bubbles formed in the measuring cylinder and water level within it ceased to change as the displacement process progressed, the S_w of the coal sample was considered to be 0. Unavoidably, owing to the limitations of the experimental conditions, some absorbed water was still present, however.

3 Results

3.1 Acoustic response of the dry samples

The types of pores and fractures in coals vary significantly, depending on the degree of coal metamorphism and deformation (Yao et al., 2010; Zhou et al., 2017; Li et al., 2020; Ju et al., 2021). This variation results in the dependence of the acoustic velocity on metamorphism, deformation (Cai et al., 2014; Li et al., 2017), and the testing direction of the coal sample (Morcote et al., 2010; Wang et al., 2016; Chen et al., 2017). The P-wave and S-wave velocity of the dry samples was tested based on the experimental steps outlined above. The relationship between V_p and V_s and the pseudo-azimuth angle, φ, is a cosine function with a period of 180°, expressed as follows:

$$V(\varphi) = A\cos(2(\varphi + \theta_0)) + B. \quad (4)$$

Taking coal sample LHG7-1 as an example, the periodic variation of V_p and V_s with the pseudo-azimuth angle is plotted in Fig. 3. As shown in this figure, the initial azimuth angle, θ_0, and the coefficients A and B were determined by curve fitting. The relative anisotropy of V_p and V_s (commonly expressed as $2A/B$) was evaluated from the wave amplitude and the average of each cosine

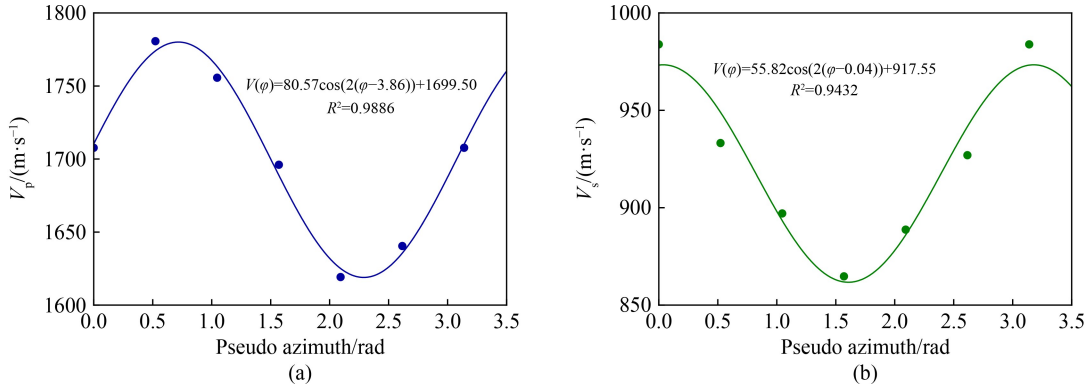

Fig. 3 Variation of the acoustic velocity with the pseudo-azimuth angle of coal sample LHG7-1. (a) P-wave; (b) S-wave.

function. The acoustic velocity and relative anisotropy of the dry samples are listed in Table 2.

3.2 Acoustic response of the gas-water saturated coal samples

3.2.1 Acoustic velocity

The V_p and V_s of each coal sample containing gas-water at different S_w were tested. The test results are shown in Table 3.

3.2.2 Relative anisotropy

To investigate the influence of gas-water saturation on the acoustic anisotropy of the coal samples, theV_p and V_s of samples LHG7-1 (low-rank primary coal), LL-ZJD (medium-rank primary coal), YQ-5K (high-rank primary coal) and GJ (medium-rank tectonic coal) were tested at

Table 2 Test results of acoustic parameters of each dry sample

Sample ID	V_p/(m·s^{-1})	V_s/(m·s^{-1})	V_p/V_s	*A*		*B*		Relative anisotropy	
				V_p	V_s	V_p	V_s	V_p	V_s
LHG7-1	1707.65	983.86	1.74	80.57	55.82	1699.50	917.55	9.48	12.17
L7	1853.85	1037.66	1.79	72.32	62.68	1892.13	1066.78	7.64	11.75
LL-LL	1931.99	1089.45	1.77	130.98	47.53	1909.72	1075.53	13.72	8.83
LL-YT	2009.65	1119.57	1.80	131.06	125.76	1905.09	1199.63	13.76	20.97
LL-ZJD	2127.75	1186.29	1.79	123.44	130.16	2169.67	1259.53	11.38	20.67
LL-SC	2364.17	1256.35	1.88	188.46	78.33	2448.00	1359.70	15.40	11.52
CC	2385.19	1267.68	1.88	134.29	61.41	2285.35	1183.59	11.75	10.38
YQ-5K	2593.36	1532.80	1.69	172.48	127.09	2451.81	1506.51	14.07	16.87
GJ	2347.41	1246.88	1.88	165.99	115.69	2459.08	1192.04	13.50	19.41

Table 3 Acoustic velocities at different S_w of coal samples

Sample ID	V_p at different S_w/(m·s^{-1})						V_s at different S_w/(m·s^{-1})					
	100%	80%	60%	40%	20%	0	100%	80%	60%	40%	20%	0
LHG7-1	2456	2090	1927	1724	1449	1423	1333	1245	1083	934	824	803
L7	2441	2148	1985	1642	1578	1502	1265	1188	1051	825	758	746
LL-LL	2595	2332	2270	1946	1791	1731	1358	1266	1159	1080	985	970
LL-YT	2657	2494	2212	2021	1927	1825	1443	1297	1263	1125	1085	985
LL-ZJD	2641	2401	2213	2133	2036	1990	1505	1343	1311	1259	1189	1150
LL-SC	2771	2585	2450	2364	2193	2148	1665	1580	1433	1353	1295	1247
CC	2622	2438	2232	2144	2076	2026	1485	1323	1282	1225	1197	1154
YQ-5K	2990	2821	2785	2706	2597	2548	1796	1704	1654	1583	1536	1514
GJ	2886	2712	2433	2176	2064	1911	1401	1357	1216	1088	1001	956

different orientations according to the test method outlined above. The corresponding relative anisotropy was then calculated by fitting the cosine function shown in Eq. (4). The calculation results are listed in Table 4.

4 Discussion and analysis

4.1 Factors influencing the acoustic response of the dry coal samples

Based on the basic physical and acoustic parameters of the dry coal samples (Tables 1 and 2), the correlation between wave velocity and the vitrinite reflectance and density of the coal samples is presented in Fig. 4. The correlation between the vitrinite reflectance and density of the coal samples and the V_p/V_s ratio and relative anisotropy is presented in Fig. 5.

As shown in Fig. 4, the V_p and V_s of the tested coal samples were linearly correlated with vitrinite reflectance and density. This finding is consistent with previous studies showing that both the P-wave and S-wave velocity increase with the density of the coal rock (Khandelwal and Ranjith, 2010; Xu et al., 2020). The V_p/V_s ratio and acoustic anisotropy are commonly used to characterize rock lithology and structural features (Allan et al., 2014; Lin et al., 2016). In this study, both the V_p/V_s ratio and relative anisotropy tended to increase with increasing vitrinite reflectance and density of the coal samples (Fig. 5), but the correlation between them was not very strong.

4.2 Acoustic parameters variation of the gas-water saturated coal samples

4.2.1 Acoustic velocity

Based on the acoustic velocity in gas-water saturated coal

Table 4 Relative anisotropies at different S_w of coal samples containing gas-water

Sample ID	Relative anisotropy of V_p at different S_w/(m·s^{-1})						Relative anisotropy of V_s at different S_w/(m·s^{-1})					
	100%	80%	60%	40%	20%	0	100%	80%	60%	40%	20%	0
LHG7-1	16.83	15.22	14.71	11.64	10.38	10.12	22.15	24.3	19.24	15.68	15.39	12.07
LL-ZJD	18.03	15.57	13.88	12.79	13.46	11.25	26.79	26.01	25.77	22.26	19.67	20.35
YQ-5K	20.98	19.21	17.33	16.98	14.53	14.07	25.04	22.65	20.52	16.7	18.73	15.46
GJ	19.77	17.44	17.03	15.58	13.87	13.39	28.86	27.48	25.87	23.69	20.46	18.39

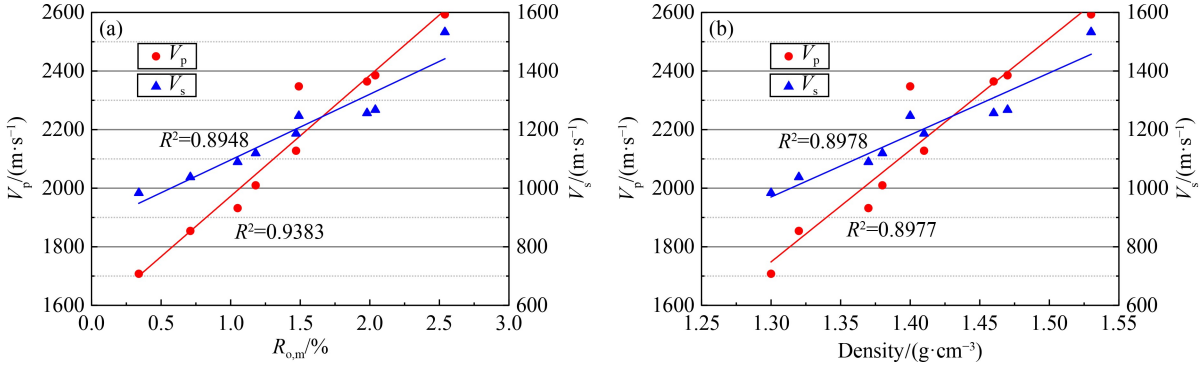

Fig. 4 Correlation of (a) vitrinite reflectance and (b) density with wave velocity of coal samples.

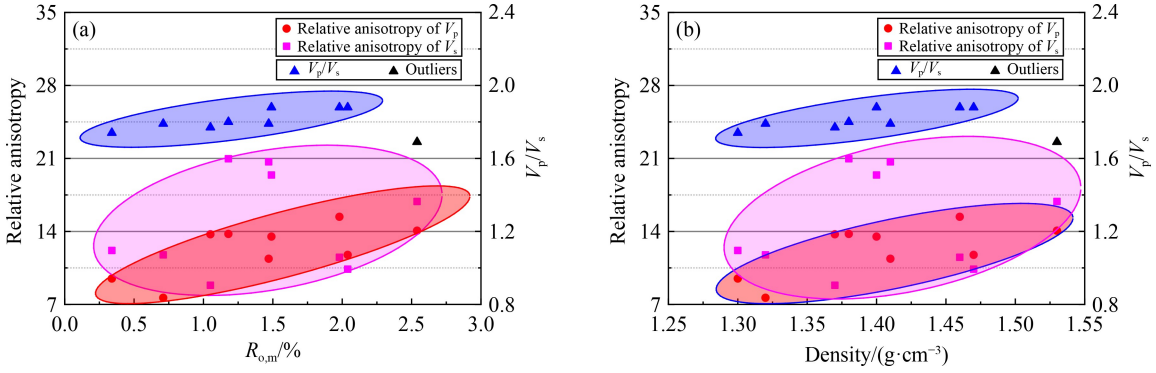

Fig. 5 Correlation of (a) vitrinite reflectance and (b) density with relative anisotropy and V_p/V_s ratio of coal samples.

samples of different S_w values (Table 3), the correlation curves of V_p and V_s with S_w and S_g were fitted for each coal sample (Fig. 6).

The presence of fluid affects the physical properties of rocks (Erguler and Ulusay, 2009; Lebedev et al., 2014). The positive correlation between the acoustic velocity and S_w in coal (which means that V_p increases exponentially with increasing S_w) was recognized through acoustic tests of coal samples with different S_w (Liu et al., 2017b; Wang et al., 2020; Dugarov et al., 2021). In this study, the P-wave and S-wave velocity gradually increased with increasing S_w. The V_s growth rate was relatively continuous with increasing S_w of the coal sample. The V_p growth rate, on the other hand, was slower for $S_w < 40\%$, and faster for $S_w > 60\%$. The comparison between the V_p and V_s of the saturated and dry coal samples shows that both the P-wave and S-wave velocity in the dry coal samples were lower than those in the fully water-saturated coal samples and higher than those in the fully gas-saturated coal samples. This may be because the confining and axial pressure loaded during the displacement experiments on the saturated coal samples caused further expansion of the samples' internal fractures.

With increasing vitrinite reflectance and density, and S_w increasing from 0 to 100%, the range of V_p and V_s increase gradually narrowed. This indicates that the greater the vitrinite reflectance and density of the coal, the weaker the influence of S_w on wave velocity, possibly due to the weaker water absorption in the coal samples at normal pressure and temperature.

The comparison between coal samples with a similar vitrinite reflectance but a different coal structure (tectonic coal sample GJ versus primary coal sample LL-ZJD) shows that with S_w increasing from 0 to 100%, the increase in the P-wave and S-wave velocity was significantly higher in the tectonic coal sample, GJ. This suggests that the S_w of the tectonic coal had a stronger influence on the acoustic waves than the S_w of the primary coal. This result can be explained by the difference in the physical parameters of the two coal samples: the tectonic coal contains developed pores and fractures, which commonly result in stronger water absorption.

4.2.2 Ratio of P-wave velocity to S-wave velocity

The V_p/V_s ratio of each coal sample at different S_w values was calculated from the acoustic velocities (Table 3). In our tests, there was no significant correlation between the V_p/V_s ratio and the vitrinite reflectance of the coal sample or the S_w of the mixed-phase fluid. However, there were significant differences between coals at different degrees of deformation: the V_p/V_s ratio of the gas-water saturated tectonic coal was higher than that of the primary coal (Fig. 7). This indicates that the V_p/V_s ratio depends on coal structure, and increases with the transformation of primary into tectonic coal (Wang et al., 2014).

4.2.3 Acoustic anisotropy variation law of coal samples containing gas-water mixed-phase fluid

The gas and water saturation (S_g and S_w, respectively) and relative anisotropy of the coal samples exhibited a linear correlation (Fig. 8). The regression analysis results for the acoustic anisotropy and S_w of the tested samples are shown in Table 5.

As shown in Fig. 8 and Table 5, the relative anisotropy of both V_p and V_s increased linearly with S_w. The relative anisotropy of V_s was stronger than that of V_p, and its growth rate with increasing S_w was higher. With increasing vitrinite reflectance and density of the coal samples, the relative anisotropy of V_p for a given S_w increased gradually. The relative anisotropy of V_s was stronger for medium-rank coal and weaker for low-rank and high-rank coals.

The comparison between the acoustic anisotropy of the tectonic coal sample, GJ, and the primary coal sample LL-ZJD showed that, at the same $S_w > 0$, the relative anisotropy of both V_p and V_s was stronger in sample GJ than in sample LL-ZJD. With increasing S_w, the relative

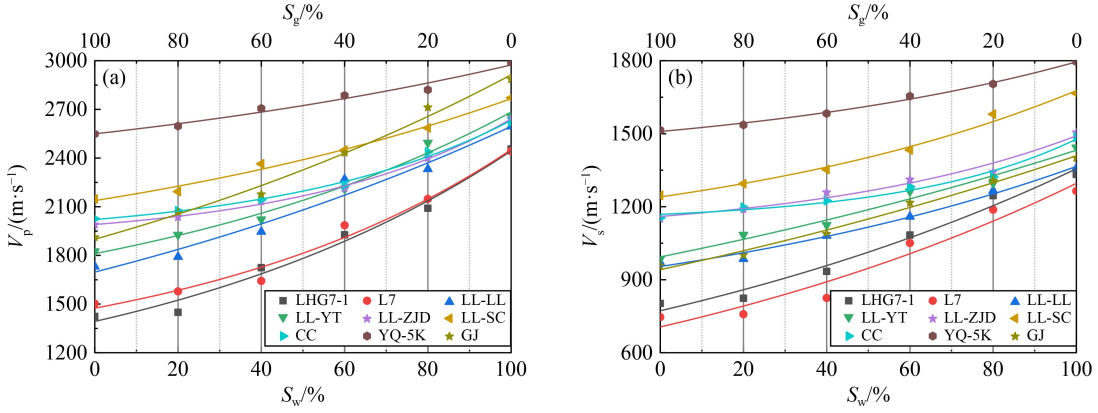

Fig. 6 Acoustic velocity variations of gas-water saturated coal samples. (a) P-wave; (b) S-wave.

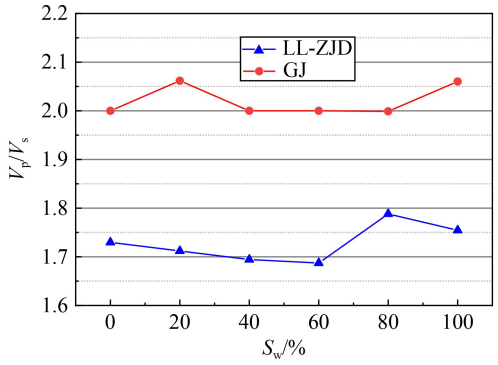

Fig. 7 Differences in V_p/V_s ratio of primary coal sample and tectonic coal sample.

anisotropy of V_p and V_s was significantly stronger, and its growth rate was also higher in GJ as compared with LL-ZJD. This suggests that the acoustic anisotropy was stronger in the tectonic coal with well-developed pores and fractures. In that coal, water absorption was stronger than that in the primary coal, and the acoustic anisotropy was more markedly influenced by S_w.

5 Conclusions

Based on the acoustic tests on dry and gas-water saturated coal samples, the differences of V_p, V_s, V_p/V_s ratio, and relative anisotropy were compared in this work. The variation law of acoustic response of dry and gas-water saturated coal samples was discussed, and conclusions were summarized as follow.

1) The acoustic velocity of dry coal samples was linearly with vitrinite reflectance and density. Meanwhile, the V_p/V_s ratio, relative anisotropy of both V_p and V_s of dry coal samples tended to increase with increasing vitrinite reflectance and density of the coal samples, but the correlation between them was not very strong.

2) The V_p and V_s of gas-water saturated coal samples increased gradually with increasing S_w and vitrinite reflectance. However, with increasing vitrinite reflectance and density, and S_w increasing from 0 to 100%, the range of V_p and V_s increase gradually narrowed. For coal samples with similar vitrinite reflectance, the V_p/V_s ratio of tectonic coals were larger than those of primary coals, and the increase rang of V_p and V_s of tectonic coal was also significantly higher when the S_w increasing from 0 to 100%.

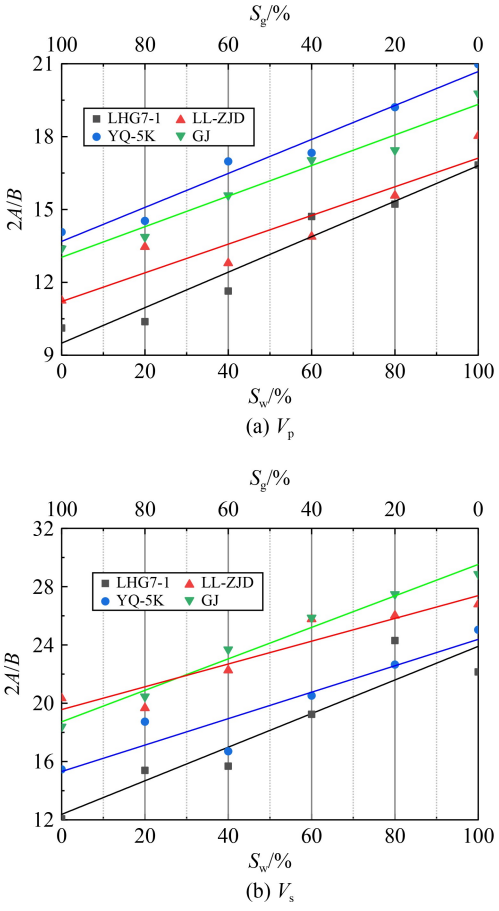

Fig. 8 Acoustic anisotropy variations of coal samples containing mixed-phase fluid.

3) The relative anisotropy of both V_p and V_s increased linearly with the S_w. For coal samples with similar vitrinite reflectance, the relative anisotropy of V_p and V_s and its growth rate of the tectonic coal was larger than that of the primary coal in general at the same S_w. This suggests that the acoustic anisotropy was stronger in the tectonic coal with well-developed pores and fractures. The anisotropy is more markedly influenced by the water saturation S_w.

Acknowledgments This research was funded by the National Natural Science Foundation of China (Grant Nos. 42130806, 41922016, 41830427 and 41772160).

Table 5 Regression analysis results of acoustic anisotropy and water saturation

Sample ID	Regression expression for $2A/B$ and S_w			
	V_p	R^2	V_s	R^2
LHG7-1	$2A/B = 0.0730S_w + 9.4971$	0.9355	$2A/B = 0.1153S_w + 12.3748$	0.8500
LL-ZJD	$2A/B = 0.0590S_w + 11.2119$	0.8436	$2A/B = 0.0907S_w + 15.3157$	0.8457
YQ-5K	$2A/B = 0.0699S_w + 13.6876$	0.9588	$2A/B = 0.0782S_w + 19.5657$	0.8551
GJ	$2A/B = 0.0629S_w + 13.0329$	0.9838	$2A/B = 0.1080S_w + 18.7257$	0.9759

References

Allan A M, Vanorio T, Dahl J E P (2014). Pyrolysis-induced P-wave velocity anisotropy in organic-rich shales. Geophysics, 79(2): D41–D53

Altindag R, Güney A (2006). ISRM suggested method for determining the shore hardness value for rock. Int J Rock Mech Min Sci, 43(1): 19–22

Banerjee A, Chatterjee R (2021). Fracture analysis using stoneley waves in a coalbed methane reservoir. Near Surf Geophys: nsg.12176

Cai Y D, Liu D M, Mathews J P, Pan Z J, Elsworth D, Yao Y B, Li J Q, Guo X Q (2014). Permeability evolution in fractured coal—combining triaxial confinement with X-ray computed tomography, acoustic emission and ultrasonic techniques. Int J Coal Geol, 122: 91–104

Chen H D, Jiang B, Chen T J, Xu S C, Zhu G Y (2017). Experimental study on ultrasonic velocity and anisotropy of tectonically deformed coal. Int J Coal Geol, 179: 242–252

Dugarov G A, Duchkov A A, Manakov A Y (2021). Acoustic properties of hydrate-bearing coal samples depending on temperature and water saturation type. Geophysics, 86(3): U31–U37

Erguler Z A, Ulusay R (2009). Water-induced variations in mechanical properties of claybearing rocks. Int J Rock Mech Min Sci, 46(2): 355–370

Feng J J, Wang E Y, Chen L, Li X L, Xu Z Y, Li G A (2016). Experimental study of the stress effect on attenuation of normally incident P-wave through coal. J Appl Geophys, 132: 25–32

Hou L L, Liu X J, Liang L X, Xiong J, Zhang P, Xie B, Li D Q (2020). Investigation of coal and rock geo-mechanical properties evaluation based on the fracture complexity and wave velocity. J Nat Gas Sci Eng, 75: 103133

Ju W, Shen J, Li C, Yu K, Yang H (2021). Natural fractures within unconventional reservoirs of Linxing Block, eastern Ordos Basin, central China. Front Earth Sci, 14(4): 770–782

Khandelwal M, Singh T N (2009). Correlating static properties of coal measures rocks with P-wave velocity. Int J Coal Geol, 79(1–2): 55–60

Khandelwal M, Ranjith P G (2010). Correlating index properties of rocks with P-wave measurements. J Appl Geophys, 71(1): 1–5

Khandelwal M (2013). Correlating P-wave velocity with the physico-mechanical properties of different rocks. Pure Appl Geophys, 170(4): 507–514

Li X C, Meng Y Y, Yang C L, Nie B S, Mao Y J, Chen X H (2017). Effects of pore structure on acoustic wave velocity of coal samples. J Nanosci Nanotechnol, 17(9): 6532–6538

Li Z T, Liu D M, Cai Y D, Wang Y P, Si G Y (2020). Evaluation of coal petrophysics incorporating fractal characteristics by mercury intrusion porosimetry and low-field NMR. Fuel, 263: 116802

Lin J Y, Hsu S K, Lin A T S, Yeh Y C, Lo C L (2016). V_p/V_s distribution in the northern Taiwan area: implications for the tectonic structures and rock property variations. Tectonophysics, 692: 181–190

Liu D M, Zou Z, Cai Y D, Qiu Y K, Zhou Y F, He S (2021). An updated study on CH_4 isothermal adsorption and isosteric adsorption heat behaviors of variable rank coals. J Nat Gas Sci Eng, 89: 103899

Liu G H, Liu Z T, Feng J J, Song Z K, Liu Z J (2017a). Experimental research on the ultrasonic attenuation mechanism of coal. J Geophys Eng, 14(3): 502–512

Liu J, Liu D M, Cai Y D, Gan Q, Yao Y B (2017b). Effects of water saturation on P-wave propagation in fractured coals: an experimental perspective. J Appl Geophys, 144: 94–103

Liu Z S, Liu D M, Cai Y D, Yao Y B, Pan Z J, Zhou Y F (2020). Application of nuclear magnetic resonance (NMR) in coalbed methane and shale reservoirs: a review. Int J Coal Geol, 218: 103261

Lupton N, Connell L D, Heryanto D, Sander R, Camilleri M, Down D I, Pan Z J (2020). Enhancing biogenic methane generation in coalbed methane reservoirs—core flooding experiments on coals at *in-situ* conditions. Int J Coal Geol, 219: 103377

Lebedev M, Wilson M E J, Vassily M (2014). An experimental study of solid matrix weakening in water-saturated Savonnières limestone. Geophys Prospect, 62(6): 1253–1265

Morcote A, Mavko G, Prasad M (2010). Dynamic elastic properties of coal. Geophysics, 75(6): E227–E234

Sharma P K, Singh T N (2008). A correlation between P-wave velocity, impact strength index, slake durability index and uniaxial compressive strength. Bull Eng Geol Environ, 67(1): 17–22

Wang G, Li J Z, Liu Z Y, Qin X J, Yan S (2020). Relationship between wave speed variation and microstructure of coal under wet conditions. Int J Rock Mech Min Sci, 126: 104203

Wang H C, Pan J N, Wang S, Zhu H T (2015). Relationship between macro-fracture density, P-wave velocity, and permeability of coal. J Appl Geophys, 117: 111–117

Wang N, Zhao S S, Hui J, Qin Q M (2017). Three-dimensional audio-magnetotelluric sounding in monitoring coalbed methane reservoirs. J Appl Geophys, 138: 198–209

Wang Y, Xu X K, Yang D Y (2014). Ultrasonic elastic characteristics of five kinds of metamorphic deformed coals under room temperature and pressure conditions. Sci China Earth Sci, 57(9): 2208–2216

Wang Y, Xu X K, Zhang Y G (2016). Ultrasonic elastic characteristics of six kinds of metamorphic coals in China under room temperature and pressure conditions. Chin J Geophys, 59(7): 2726–2738

Xu X M, Chang Y Q, Zhao W W, Liu H, Lv C, Wang H N, (2020). Experimental study of correlating the acoustic velocity and the physical-mechanical properties of coal under varied stress based on clean coal energy development concept. Fresenius Environ Bull, 29(8): 6843–6852

Yao Y B, Liu D M, Cai Y D, Li J Q (2010). Advanced characterization of pores and fractures in coals by nuclear magnetic resonance and X-ray computed tomography. Sci China Earth Sci, 53(6): 854–862

Zhang X D, Li P P, Yang Y H, Du Z G (2017). Characteristics of P-wave and S-wave times and their relationship with Young's modulus of coals with different degrees of deformation. Arab J Geosci, 10(4): 75

Zhang Z H, Wang E Y, Liu X N, Zhang Y H, Li S J, Khan M, Gao Y K (2021). Anisotropic characteristics of ultrasonic transmission velocities and stress inversion during uniaxial compression process. J Appl Geophys, 186: 104274

Zhao T B, Gu X B, Guo W Y, Gong X F, Xiao Y X, Kong B A, Zhang C G (2021). Influence of rock strength on the mechanical behavior and P-velocity evolution of coal-rock combination specimen. J Mater Res Technol, 12(1): 1113–1124

Zhou S D, Liu D M, Cai Y D, Yao Y B, Li Z T (2017). 3D characterization and quantitative evaluation of pore-fracture networks of two Chinese coals using FIB-SEM tomography. Int J Coal Geol, 174: 41–54